1

# Modelling Shear Bands in a Volcanic Conduit:

# Implications for Over-Pressures and Extrusion-Rates.

4

5

Alina J. Hale[1] & Hans-B. Mühlhaus[1]

8

[1]Earth Systems Science Computational Centre (ESSCC)

Australian Computational Earth Systems Simulator (ACcESS)

The University of Queensland

QLD 4072

Australia

14

Email: Alina Jane Hale - alinah@esscc.uq.edu.au

Email: Hans-Bernd Mühlhaus – h.muhlhaus@uq.edu.au

17

Corresponding author: Alina Jane Hale

Tel: +61 (0)7 3346 4110, Fax: +61 (0)7 3346 4134, E-mail alinah@esscc.uq.edu.au

Earth Systems Science Computational Centre (ESSCC), Australian Computational Earth Systems

Simulator (ACcESS), The University of Queensland , Brisbane, QLD 4072, Australia

22

23 **Abstract**

24 Shear bands in a volcanic conduit are modelled for crystal-rich magma flow using simplified conditions

25 to capture the fundamental behaviour of a natural system. Our simulations begin with magma

26 crystallinity in equilibrium with an applied pressure field and isothermal conditions. The viscosity of the

27 magma is derived using existing empirical equations and is dependent upon temperature, water content

28 and crystallinity. From these initial conduit conditions we utilize the Finite Element Method, using axi-

29 symmetric coordinates, to simulate shear bands via shear localisation. We use the von Mises visco-

30 plasticity model with constant magma shear strength for a first look into the effects of plasticity. The

31 extent of shear bands in the conduit is explored with a numerical model parameterized with values

32 appropriate for Soufrière Hills Volcano, Montserrat, although the model is generic in nature. Our model

33 simulates shallow (up to approximately 700m) shear bands that occur within the upper conduit and

34 probably govern the lava extrusion style due to shear boundaries. We also model the change in the over-

35 pressure field within the conduit for flow with and without shear bands. The pressure change can be as

36 large as several MPa at shallow depths in the conduit, which generates a maximum change in the

37 pressure gradient of 10's of kPa/m. The formation of shear bands could therefore provide an alternative

38 or additional mechanism for the inflation/deflation of the volcano flanks as measured by tilt-metres.

39 Shear bands are found to have a significant effect upon the magma ascent rate due to shear-induced flow

40 reducing conduit friction and altering the over-pressure in the upper conduit. Since we do not model

41 frictional controlled slip, only plastic flow, our model calculates the minimum change in extrusion rate

42 due to shear bands. However, extrusion rates can almost double due to the formation of shear bands,

43 which may help suppress volatile loss. Due to the paucity of data and large parameter space available for

44 the magma shear strength our model results can only allow for a qualitative comparison to a natural

45 system at this stage.

46

47

48    **Key words:**

49    Magma flow

50    Finite element method

51    Shear bands

52    Lava dome

53    Computational volcanology

54    Soufrière Hills Volcano

55

56  **1. Introduction**

57  Lava domes form when the extruded lava is so viscous it cannot flow freely away from the vent. Such

58  structures can grow slowly for many weeks to years without being a threat to the surrounding

59  population, but occasionally, a lava dome may collapse or explode. The main risk from collapse events

60  are pyroclastic flows, concentrated dispersions of hot volcanic fragments that move rapidly down the

61  volcano flanks in response to gravity [1]. Collapse events are a regular occurrence on Soufrière Hills

62  Volcano (SHV), Montserrat, and can take the form of repeated destruction and reconstruction of the

63  dome, often with the locus of new growth switching over time.

64

65  Lava dome emplacement morphology ranges from near solid structures to more fluid flows, and is

66  dominated by the degree of magma crystallisation [2, 3]. Crystal growth in intermediate composition

67  magma occurs primarily due to the exsolution of volatiles, due to a decrease in pressure during ascent

68  that acts to lower the liquidus temperature of the melt. Consequently, magma undergoes profound

69  rheological stiffening during ascent, which can change the magma from a Newtonian fluid into a hot

70  crystalline solid with only small amounts of residual melt [4]. Crystallisation is also time-dependent and

71  for SHV, and lava domes generally, the morphology of the dome exhibits a high degree of correlation

72  with the lava extrusion rate [2]. At the lowest extrusion rates lava is highly crystalline (85 to 95% solid

73  fraction) within the upper conduit. During these conditions lava dome growth occurs in a predominantly

74  extrusive (exogenous) fashion, producing crystal-rich structures such as spines and whalebacks [2]. At

75  higher extrusion rates the magma has less time to crystallize in the conduit, resulting in more fluid-like

76  behaviour including intrusive (endogenous) inflation and exogenous low aspect ratio flows.

77

78    During exogenous dome growth, lava is extruded directly to the free surface of the dome, implying some

79    form of internal structure capable of channelling the magma. During emplacement the lava often

80    extrudes in a stick-slip manner along curved structures, interpreted as ductile shear boundaries,

81    suggesting that the conduit wall provides the main detachment surface. Spines, whalebacks and other

82    crystal-rich exogenous structures commonly exhibit sub-parallel groves running along their length

83    parallel with the direction of extrusion, that indicate some form of shear process [4]. Observational

84    evidence of these structures also identifies cataclasites, suggesting the development of brittle shear

85    bands [5]. The lava extrusion style is therefore to some degree controlled by shear bands, their presence

86    being fundamental in crystal-rich exogenous emplacement.

87

88    Three types of seismic signal are commonly observed during silicic volcanic eruptions: Volcano-

89    Tectonic (VT) events thought to be indicative of rock fracture, Long-Period (LP) events characterized

90    by their harmonic signature and interpreted as oscillations in a fluid-filled resonator, and Hybrids which

91    have a high-frequency onset (VT) followed by a low-frequency ringing (LP) [6, 7]. For SHV, the depth

92    at which these seismic signals occur is anywhere between the free surface and 3000m below it [8]. VT

93    events represent the deeper conduit system and spikes in activity have generally been linked to

94    significant changes in eruption activity, although they are more commonly recorded during periods of

95    dormancy [9]. Hybrid and LP events represent upper conduit and dome processes, commonly with the

96    source location remaining relatively stable over-time [9]. For SHV LP seismicity is calculated to

97    originate approximately 1500 m below the surface of the dome [10].

98

99    Cyclic behaviour at SHV during 1997 was observed for seismicity, deformation of the volcano flanks as

100   recorded by tilt-meters, as well as lava dome growth. During this period cycles ranged from 4 – 36 hours

101    (not including the Vulcanian explosion cyclic events) [3, 11, 12]. During a typical (4 − 36 hours) cyclic

102    period on SHV, lava dome growth would stagnate, as measured by the seismic network signifying the

103    accompanying rockfall activity from the dome was reduced [1]. A reduction in the lava extrusion rate is

104    indicative of crystal growth in the upper conduit, the time-scales of which are comparable to the

105    deformation cycles, leading to the formation of an impeding dense viscous plug [11]. Pressurisation of

106    magma and gas under the viscous plug can then result in the inflation of the volcano flanks. An

107    acceleration in extrusion rate, observed by an increase in the amount of rockfalls from the advancing

108    lava, signifies the formation of a new pathway for the lava and the removal of the viscous plug [2]. This

109    permits the pressure in the upper-conduit to decrease, leading to the deflation of the volcano flanks.

110    Typically dome growth is more pronounced at the peak of volcano flank tilt deformation and during

111    deflation, commonly with extrusion rates approximately doubling and lava extrusion being

112    accommodated by slip on ductile shear faults [3, 12]. The volcano flank deflations were generally more

113    rapid than flank inflation, and hybrid earthquakes were observed to coincide with the point at which

114    volcano flank inflation started to decelerate (the point of inflexion), suggesting that seismicity may be

115    initiating the depressurisation process [13].

116

117    The above evidence, along with additional observational data [5], has led some research groups to

118    postulate that hybrid and LP seismic events originate from stick-slip processes along the conduit margin

119    [10].  Shear bands, as observed at the surface of the dome during cyclic activity, could generate such

120    stick-slip behaviour, suggesting that shear bands could penetrate to the depths where LP seismicity

121    originates. Using an isotropically pressurised conduit model [14], an elastic half-space model [12], or

122    shear stresses at the wall of the conduit [15], the depth of the pressure source is calculated to be less than

123    1000 m below the surface of the dome for SHV. Since the depth of LP events is approximately 1500 m

124    below the surface of the dome, this means that the tilt and seismic hypocentres don't appear to correlate,

125    however the calculated depths are strongly model dependent.

126

127    We develop a visco-plastic axi-symmetrical Finite Element Method (FEM) model to simulate the

128    generation of shear bands, localised regions of high strain, in a conduit via shear-localization. The

129    formation of a zone or band of localised shear along the conduit wall occurs within our conduit domain

130    when the material enters the plastic limit, i.e. when the shear stress experienced equals the shear strength

131    of the magma. We neglect any potential frictional slip after shear bands have been generated,

132    considering only plastic flow and therefore the minimum change in extrusion rate. We neglect the

133    influence that bubbles have upon the viscosity and density, which may alter the flow properties. We also

134    neglect departures from isothermal conditions and the evolution of shear bands once they form, instead

135    considering the slow mode components of lava rheology, making the assumption that the timescales for

136    shear band evolution occur more rapidly than the rheology can change. Instead, we focus our attention

137    on a magma crystallinity in equilibrium with the pressure field and the influence this has upon viscosity

138    and shear stress, which is found to be more significant than for bubbles for this style of volcanism [16,

139    17]. For this paper we use constant magma shear strength because it is unknown which constitutive

140    relationship controls the mode of deformation at depth. This means that the extent of the shear bands is

141    controlled by the magma shear stress, which is effectively governed by the viscosity. Our model is

142    intended to be simplified to capture the fundamental behaviour of a natural system, such as changes in

143    extrusion rate and pressure. In section 2 we briefly discuss existing models that consider shear bands in

144    conduit flow. We follow this with the description of our conduit model in section 3, including the field

145    equations and initial conditions used. Section 4 provides results from our model and in section 5 we

146    discuss these results.

147

148    **2. Existing Models**

149    Modelling efforts have been limited by the complexities of the magma rheology, for which no complete

150    mathematical model currently exists [18]. Costa [17] recently developed an advanced model for the

151    viscosity of magma containing very high solid fractions, although this model remains Newtonian.

152    Existing numerical models have offered important insights into the fundamental characteristics of lava

153    flow in a conduit due to gas exsolution and crystallisation and how this may promote cyclic behaviour.

154    Melnik and Sparks [18 - 21] conduit models demonstrate that the major flow regimes depend upon the

155    relative time scales of magma ascent and crystallisation, and that some cyclic behaviour can be

156    attributed to the time-scales involved with crystallisation kinetics. The observation of complex

157    oscillatory behaviour in the high-pressure extrusion of industrial polymer melts led Denlinger and

158    Hoblitt [22] to develop a simple dynamic model for conduit flow. They model compressible magma

159    flow though a cylindrical conduit undergoing stick-slip motion to extract characteristic oscillatory time-

160    periods, and relate this to the cyclic periods experienced by silicic volcanoes. While Wylie et al. [23]

161    modelled volatile exsolution as magma nears the surface, the corresponding increase in magma viscosity

162    within an elastic medium, and how this promotes oscillatory flow. In all these models the oscillatory and

163    seismic behaviour is related to the magma flow instability. However, none of the models consider the

164    lateral variations across the conduit which will modify the flow properties and promote the development

165    of shear bands [24, 25].

166

167    Neuberg et al. [10] combined seismological clues, field evidence and numerical modelling to suggest a

168    trigger mechanism for LP seismicity based upon the brittle failure of magma in the glass transition. They

169    model magma flow in a conduit using the FEM. Shear bands develop at the conduit wall where loss of

170 heat and gas is modelled, consequently resulting in a high viscosity gradient. Although they base their

171 model upon the SHV, they use a very low crystallinity of 30% and this means they have to rely upon

172 very high extrusion rates to force the generation of shear bands to appropriate depths. Gonnermann and

173 Manga [26] use bubble growth and plastic failure to model the point at which magma fragmentation

174 occurs within a conduit and the influence it has upon the resulting eruption style. For their model they

175 are primarily interested in how magma melt and bubbles control viscous shearing, but do not specifically

176 consider the depth that fragmentation (intense shear) occurs, or how it then changes the extrusion rate or

177 pressure within the conduit. This is our motivation, and as for Neuberg et al. [10] and Gonnermann and

178 Manga [26] we use an empirical well-studied viscosity and constant magma shear strength for a first

179 look into the effects of plasticity.

180

181 **3. Conduit Model**

182 We model the conduit as a vertical cylinder of uniform radius between the magma chamber and the

183 volcano free surface, as shown in Figure 1. The conduit is 15 metres in radius and has a length of 5km

184 [27]. Magma ascent is driven by an over-pressure existing within the magma chamber, defined as the

185 total pressure minus magma-static pressure, and the pressure at the free surface is atmospheric. Model

186 equations are discussed in this section and Table 1 lists the parameters used in the model.

187

188 [Location of figure 1]

189 [Location of table 1]

190

191 **3.1Momentum Equations**

192    Magma is modelled as an isotropic, incompressible viscous fluid. The relationship between the

193    deviatoric part of the stress tensor $\sigma'_{ij}$ , and the symmetric part of the velocity gradient or stretching $D'_{ij}$,

194    reads:

195

196    $\sigma'_{ij} = 2\eta D'_{ij}$ ,  $i, j = (1,2,3)$ ,                                                    (1)

197    where

198    $$\sigma'_{ij} = \sigma_{ij} + P\delta_{ij} \quad and \quad P = -\frac{1}{3}\sigma_{kk},$$
$$D'_{ij} = D_{ij} - \frac{1}{3}D_{kk}\delta_{ij}.$$
                                                                                                       (2)

199    Here $\sigma_{ij}$ are components of the stress tensor, $\eta$ the viscosity, $\delta_{ij}$ is the Kronecker delta and $P$ the

200    pressure. In general the viscosity depends on the pressure, temperature and other state variables. Here

201    we focus on the dependency of $\eta$ on the crystal content as described in sections 3.4 and 3.5. We also

202    assume that any dilatancy effects associated with the crystallisation processes do not affect the

203    qualitative features of the flows considered here; i.e. we assume:

204    $D_{jj} = div\,\mathbf{v} = 0$ ,                                                                   (3)

205    where $\mathbf{v}$ is the velocity vector. The stress-equilibrium equations in axi-symmetrical coordinates, read,

206    $$\begin{aligned}(r\sigma_{rr})_{,r} + r\sigma_{rz,z} - \sigma_{\theta\theta} + rf_r = 0 \\ r\sigma_{zz,z} + (r\sigma_{rz})_{,r} + rf_z = 0\end{aligned}$$                                  .    (4)

207

208    where $f$ is the body force and $r$ is the radial coordinate. Insertion of equations 1 and 2 into 4 yields the

209    equations of motion in the following form:

210

211
$$\left(r\left(2\eta v_{r,r} - P\right)\right)_{,r} + r\left(\eta(v_{r,z} + v_{z,r})\right)_{,z} - 2\eta\frac{v_r}{r} + P + rf_r = 0$$
$$r\left(2\eta v_{z,z} - P\right)_{,z} + \left(r\eta(v_{r,z} + v_{z,r})\right)_{,r} + rf_z = 0.$$
(5)

212

### 3.2 Generating Shear Bands

214    Shear bands are weak regions stressed under high strain rates that are prone to failure. Localized shear

215    bands form if the underlying flow or deformation experiences a particular type of instability in the

216    constitutive relationship [28]. This instability expresses itself mathematically as a change in the type of

217    the tangential boundary value problem. In pressure-sensitive materials the instability may arise because

218    of a mismatch between the pressure sensitivity and the dilatancy factor and/or strain softening, for

219    example due to micro-cracking. Another important shear-band generating mechanism is related to shear

220    heating and thermal feedback due to a strongly temperature-dependent viscosity. However, this

221    mechanism is generally only relevant for high Péclet number flows (adiabatic shear banding) and is not

222    likely to be important in our study due to the low flow rates experienced at SHV [25]. Model results are

223    extremely mesh sensitive since the thickness of shear bands is undetermined in standard continuum

224    models. Strategies to overcome this ill-posedness have been developed mainly by the engineering

225    community [29]. Here we accept this mesh sensitivity so that the shear band width will be set by the

226    length scale provided by the discretisation scheme, i.e. the characteristic element width, which equals

227    the thickness of shear bands observed at SHV [4].

228

229  Magma flow rates can be highly variable due to complex feed-back processes such as time-dependent

230  crystallisation [19]. However we need an initial crystallinity, pressure and viscosity within our conduit

231  from which to initialise our model. The simplest starting point is to assume that the magma is initially

232  stationary, and that the crystal content is in equilibrium with a pressure field. Stationary magma also

233  implies that no shear bands currently exist within the conduit at the start of the simulation. From this

234  initial magma state we need to initiate flow by changing the pressure field. Over time-scales associated

235  with magma ascent in the conduit, magma chamber key variables such as over-pressure are likely to be

236  approximately constant due to its large volume with respect to the lava-dome and conduit. Since our

237  model is not transient at this stage we need to make the necessary simplification that a rapid over-

238  pressure change occurs that is large enough to force magma flow and to generate shear bands. A

239  significant and rapid pressure change within the conduit can be achieved by removing a flow-inhibiting

240  lava dome, existing at the conduit exit, by means of a collapse event. Therefore our model begins with a

241  pressure field that represents a lava dome at the conduit exit, providing a resisting pressure equal to the

242  magnitude of the over-pressure in the magma chamber. The initial pressure gradient from which to

243  evaluate the magma properties in the conduit for one simulation thus comprises of a component from the

244  magma-static pressure, plus a constant over-pressure from the weight of the lava dome. Mathematically

245  we instantaneously remove the dome and set the conduit exit pressure to be equal to atmospheric

246  pressure. The over-pressure existing within the magma chamber can then be transferred to the magma in

247  the conduit enabling flow. The velocity and pressure fields within the conduit are then calculated

248  iteratively, using the initialised viscosity field and conduit exit and magma chamber pressures as

249  boundary conditions.

250

251    The largest dome recorded at SHV was approximately 1116m above sea level, and following a collapse

252    event the deepest it excavated into the crater was approximately 700m a.s.l., resulting in a dome collapse

253    of approximately 400m [30]. This, and the estimated maximum tensile strength of the surrounding

254    country rocks of 20 MPa provides an upper limit for the pressure change in our model [31]. The

255    assumption of a magma crystallinity in equilibrium with the pressure field is not likely to be appropriate

256    during periods of sustained magma flow due to crystallisation kinetics [25]. However the largest strain-

257    rates and shear stresses are likely to be at the conduit walls due to a no-slip boundary condition. At the

258    conduit wall, where magma is stationary, the crystal volume fraction and water content in the magma

259    will be in equilibrium with the applied pressure. Hence the viscosity field along the conduit wall, where

260    shear bands form, would not be expected to change much for transient flow from our unsteady model.

261

262    **3.3 Temperature**

263    The low thermal conductivity of magma means that the temperature will not change significantly along

264    the length of the conduit, enabling us to assume the magma is in thermal equilibrium. The temperature

265    of the magma and the conduit walls in our models is set to be 1123°K [32] justified by assuming the

266    eruption is long-lived, the case for SHV, and therefore the conduit walls have been pre-heated. We

267    assume that shear bands form instantaneously so that isothermal conditions prevail. Temporal offsets

268    that may affect the flow; i.e., shear heating can further destabilize the flow once shear bands form, but

269    this effect will be secondary to the onset of shear bands.

270

271    **3.4 Physical Properties of Magma**

272    Magma contains crystals, melt and bubbles that vary in proportion during flow and ascent in the conduit.

273    Variations in the proportions of liquid and non-liquid components will modify the viscosity. The role of

274 bubbles in the magma in the simulation is ignored because its influence upon the viscosity is weak, a

275 maximum change in viscosity of approximately 75% [33] and for high viscosity dome forming eruptions

276 this value is likely to be much lower [34]. Our model focuses upon representing the crystal volume

277 fraction characteristics of the magma since this has by far the strongest influence upon the magnitude of

278 the effective viscosity, potentially increasing it to over 4 orders of magnitude [2, 17, 20, 33]. By

279 assuming the maximum crystal volume fraction possible in the magma, our model can be considered to

280 be an end-member scenario, reflecting very slow magma ascent rates, and will generate the deepest

281 shear bands owing to the highest viscosity within the conduit and the highest over-pressures required to

282 force flow.

283

284 For SHV the crystallinity in the magma chamber is calculated to be 35 to 45 vol. % phenocrysts and 15-

285 20 vol. % microphenocrysts [4] giving a total crystallinity between 50 and 65%. We assume an initial

286 crystallinity of 60 vol. % at the conduit entrance (Fig. 1). The degree of crystallisation is modelled by

287 considering the effective liquidus temperature $T_{liq}$ which changes due to the progressive chemical

288 change of the melt (Eqn. 6).

289

290 $$T_{liq} = a_T + b_T \ln(P) + c_T \ln(P)^2 + d_T \ln(P)/P^2, \quad\quad (6)$$

291

292 with the coefficients $a_T, b_t, c_T, d_T$ as given by Melnik and Sparks [21] and listed in Table 1. The

293 equilibrium crystallinity $\phi_{eq}$ in the melt phase is given by (Eqn. 7):

294

295 $$\phi_{eq} = \frac{A(P)(T - T_{liq}(P))}{B(P) - T}, \qu\quad (7)$$

296

297     where $A(P)$ and $B(T)$ are functions of the pressure and are described by Melnik and Sparks [21] and $T$

298     is the temperature. The melt viscosity of the magma is calculated using an empirical equation developed

299     by Hess and Dingwell [18] (Eqn. 8), where the water content, the primary volatile, is $c = \alpha_s \sqrt{P}$ with

300     $\alpha_s$ the solubility coefficient:

301

302     $$\log \eta_m = -3.545 + \left( 0.833 \ln c + \frac{9601 - 2368 \ln c}{T - \left(195.7 + 32.25 \ln c\right)} \right). \tag{8}$$

303

304     The total viscosity is calculated using the equation presented in Melnik and Sparks [21] (Eqn 9)

305     where $\phi = \phi_{eq}$:

306

307     $$\eta = \theta(\phi)\eta_m \tag{9}$$

308     $$\log\left( \theta(\phi) \big/ \theta_0 \right) = \left( \arctan\left(\xi(\phi - \phi_0)\right) + \pi / 2 \right)$$

309

310     Equation 9 contains the coefficients $\theta$ and $\xi$, and $\phi_0$ is the critical crystal fraction, and the values used

311     are given in Table 1. For our model, this gives a viscosity from $5 \times 10^5$ Pa s at the magma chamber up to

312     $4 \times 10^{10}$ Pa s at the conduit exit, depending upon the magma chamber pressure used.

313

314     **3.5 Magma shear strength**

315     The shear strength provides a limit to the acceptable stress states in a material. Laboratory experiments

316     show that the critical stress at the onset of yield is a function of pressure, temperature, strain, strain-rate,

317    porosity and sample size [36]. Therefore the physical properties of the magma are likely to affect the

318    yield characteristics of the magma. For example, if the magma has only small amounts of crystals then

319    the magma may yield in a ductile way as observed for metals. Whilst for cool brittle magma,

320    deformation is localized along micro-fractures that amalgamate into a shear surface at failure [4]. Since

321    we do not have knowledge of the yield mechanism along the conduit length we must focus on the

322    simplest scenario, a constant magma shear strength with a magnitude obtained from the brittle-ductile

323    criteria for glasses. For a first look into the effects of plasticity we use the von Mises visco-plastic model

324    with the yield criterion given by equation 10, where $F$ designates the yield function, $\tau = \sqrt{1/2\sigma'_{ij}\sigma'_{ij}}$ is

325    the equivalent shear stress and $\tau_S$ is the magma shear strength. Prior to yielding the material deforms

326    linearly (i.e. Newtonianly), and once the shear strength has been reached some fraction of the

327    deformation will be permanent and non-reversible with plastic flow along a shear band.

328

329    $F = \tau - \tau_S \leq 0$ .                                                              (10)

330

331    For an illustration how the criterion (Eqn. 10) works, consider simple shear with a prescribed

332    monotonically increasing strain rate. At sufficiently low strain rates the shear stress is below the magma

333    shear strength $\tau_S$ . As the strain rate increases the shear stress will eventually reach $\tau_S$ . It is non-physical

334    for $\tau - \tau_S > 0$, that is to have a stress exceeding the magma shear strength, thus even if the strain rate is

335    increased the shear stress will remain constant with $\tau = \tau_S$ . Hence, shear bands are less likely to develop

336    as the magma shear strength increases and the driving force of the process controlling the magnitude of

337    the shear stress remains unaltered, because higher shear stresses are required to permit the magma to

338    enter the plastic regime. To model plastic flow we define an effective viscosity $\eta_{eff} = \min[\eta, \eta_S]$ in the

339    solution of the velocity-pressure problem (Eqn. 5), $\eta$ is the pre-yield viscosity (Eqn. 9) and $\eta_S = \tau_S / \dot{\gamma}$,

340    where $\dot{\gamma}$ is the equivalent strain-rate, i.e. $\dot{\gamma} = \sqrt{2 D_{ij} D_{ij}}$. Since $\dot{\gamma}$ is unknown initially the solution has to

341    be determined iteratively. The definition of $\eta_{eff}$ ensures that after enough iterations $\tau - \tau_S \leq 0$

342    everywhere. Although the non-linear problem is solved iteratively using a secant rather a tangent

343    method, the character and the properties of the solution is determined by the properties of the tangential

344    problem [37]. During the iterations the plastic zone typically narrows and lengthens continuously until it

345    is localized in a band of approximately one element size width along the conduit wall. In this particular

346    case the plastic zone coincides with the domain occupied by the shear band.

347

348    Table 2 gives values for $\tau_S$ from the literature. Apparent from table 2 is that the magma shear strength is

349    not well constrained. Some of this scatter is because the physical properties of semi-molten magma are

350    hard to measure given the technical difficulties involved in deforming samples of lava at the high

351    temperatures, pressures and strain rates that occur within natural systems.

352

353    [Location of table 2]

354

355    **4. Results**

356    The axi-symmetrical equations (3-5) are solved using the parallelized FEM based PDE solver eScript

357    and the FE library Finley [38]. More details on the solution process for the velocity and pressure fields

358    can be found in [39]. The axi-symmetric cylindrical conduit is discretised using 5000 x 15 elements with

359    quadratic shape functions (8 nodes per element) in conjunction with 4 point Gauss integration for the

360    element matrices.

361

362 **4.1 Shear band generation**

363 Figure 2 shows results from one simulation with magma shear strength of $2\times10^5$Pa and a magma

364 chamber pressure of 132.2 MPa, which required a pressure change of 14.7MPa at the conduit exit. From

365 left to right in figure 2 we produce plots of velocity in $X_3$-axis, strain-rate, shear stress, and shear stress

366 divided by the magma shear strength (effectively the plasticity). Where the shear stress divided by the

367 magma shear strength is exactly equal to unity, shear bands will form. This results in a narrow band one

368 element wide flush against the conduit wall, and for this simulation corresponds to a shear band length

369 of 413.5m. In all the models presented, shear bands form a continuous band between the conduit exit

370 and the maximum depth of the shear band directly against the conduit wall. This is due to the effective

371 viscosity increasing towards the conduit exit (Fig. 3) and the magma shear strength having a constant

372 value.

373

374 [Location of figure 2]

375

376 **4.2 Shear band length.**

377 Figure 4 shows the length that shear bands penetrate into the conduit for two different magma shear

378 strengths over a range of magma chamber pressures, from 2.4MPa to 25.4MPa. Using a magma shear

379 strength of $10^6$ Pa the result was that no shear bands form in the conduit over the magma chamber

380 pressures used. By reducing the magma shear strength we can force shear bands to form, because it

381 effectively decreases the shear-stress required before the magma enters the plastic regime. For a magma

382 shear strength of $5\times10^5$Pa shear bands develop to a maximum depth of 130 metres, whilst for a magma

383 shear strength of $2\times10^5$Pa shear bands develop to a maximum depth of 703 metres. The length of the

384 shear band within a conduit will depend upon the magma viscosity and the driving pressure. Although a

385    magma shear strength change from $2x10^5$Pa to $5x10^5$Pa is only small, the length that shear bands form to

386    is significantly affected because the viscosity changes occurs most dramatically in the upper conduit.

387    Figure 3 shows the relaxed Newtonian viscosity along the length of the conduit at the start of the

388    simulation as well as the crystal volume fraction of the magma with depth. Figure 4 also shows that

389    shear bands will not form within the conduit for magma chamber pressure below approximately 130MPa

390    (an over-pressure of 12MPa) for a magma shear strength of $5x10^5$Pa, whilst for a magma shear strength

391    of $2x10^5$Pa shear bands only form for magma chamber pressures exceeding 120MPa (i.e. an over-

392    pressure of 2MPa).

393

394

395    [Location of figure 3]

396    [Location of figure 4]

397

398

399    For low magma chamber pressures, corresponding to an initially small change in pressure at the conduit

400    exit, the viscosity in the upper conduit will be relatively large (Eqns. 7 - 9). However, due to the low

401    extrusion rate (a consequence of the lower over-pressure), shear bands will not penetrate deep into the

402    conduit. For increasing magma chamber pressures, i.e. increased dome retarding pressures, the viscosity

403    in the upper conduit will decrease since crystallinity is a function of pressure. However, a higher over-

404    pressure will result in a higher extrusion rate allowing the shear band length to increase with increasing

405    magma chamber pressure. The length that shear bands penetrate into the conduit tends towards an upper

406    limit, most clearly shown for a magma shear strength of $5x10^5$Pa (Fig. 4), due to the viscosity decreasing

407    with increasing depth within the conduit (Fig. 3).

408

409  **4.3 Shear band influence upon extrusion rate.**

410  Shear bands are likely to effect magma ascent rates by reducing conduit friction and consequently the

411  large over-pressures required to extrude highly crystalline silicic magmas. We calculate the extrusion

412  rate for magma flow with no shear bands in the conduit (i.e. Hagen-Poiseuille flow), assuming the

413  magma does not enter the plastic regime. For the same magma chamber pressure we calculate the

414  extrusion rate for magma flow in the conduit with shear bands permitted to form. Since our model

415  ignores a possible elastic-brittle contribution to the rheology, frictional slip can not be modelled. As a

416  consequence we model the minimum change in extrusion rate due to plastic deformation only.

417

418  [Location of figure 5]

419

420  Figure 5 shows the modelled extrusion rate (a) and its relative change (b) with and without shear bands

421  in the conduit, plotted against the pressure in the magma chamber. For a magma shear strength of

422  $5 \times 10^5$ Pa shear bands can penetrate to depths of 130 m, which results in a maximum change in extrusion

423  rate of approximately 3%. Whilst for a magma shear strength of $2 \times 10^5$ Pa, at the highest magma

424  chamber pressures shear bands reach a depth of 703 m resulting in a change in the extrusion rate of

425  almost 100%. Transitions between effusive and explosive volcanic activity are essentially controlled by

426  volatiles. The ability of gas trapped within the magma melt, from exsolved volatiles, to expand or escape

427  by permeable flow will determine if the ascending magma will be effusive or explosive. Slowly

428  ascending magma has time to release this build-up of gas resulting in highly degassed effusive magma.

429  However, magma ascending rapidly may not be able to release the build-up of gas, and this may result in

430  explosive activity. Gonnermann and Manga [26] suggest that fragmentation at the conduit wall, from

431  localised regions of high strain, may act to inhibit explosive behaviour due the enhanced permeability

432    from the fracture network that develops. However, cyclic activity in 1997 at SHV produced numerous

433    Vulcanian explosions with each episode preceded by a large dome collapse [40]. These collapse events

434    may have forced the generation of shear bands in the upper conduit due to a large change in pressure as

435    shown by our models. If these shear bands form rapidly enough, instantaneously in our visco-plastic

436    model, the enhanced extrusion rate due to shear band formation may be large enough to prevent volatiles

437    exsolving effusively. This may result in a competition between the processes of enhanced permeability

438    from fragmentation and reduced gas loss due to enhanced extrusion rates. Therefore deep shear bands

439    may be more likely to promote explosive activity due to a potentially large increase in extrusion rate.

440

441    The relative increase in extrusion rate due to the formation of shear bands is non-linear (Fig 5b). This is

442    due to two processes, first the length of shear bands tends towards an upper limit due to the decrease in

443    viscosity with depth in the upper conduit (Fig. 3). Second, at increasing depths in the conduit the

444    viscosity is lower, which will result in a smaller decrease from Newtonian to shear viscosity, meaning

445    that the conduit resistance change is not as significant. At low magma chamber pressures (<130MPa) the

446    extrusion rate is at the low end of the observed range for SHV (<0.5$m^3s^{-1}$). Lava is commonly extruded

447    along shear surfaces at these extrusion rates due to the high degree of crystallinity in the magma. Since

448    the generation of shear bands at these magma chamber pressures have a relatively minor influence upon

449    the extrusion rate (changing it by up to 40%) this suggests that shear bands forming at this extrusion rate

450    may be relatively stable and the crystal content will not vary significantly due to crystallisation kinetics

451    [20].

452

453

454    **4.4 Shear band influence upon the over-pressure field**

455 Cyclic inflation and deflation of the flanks of the volcano as recorded by tilt-meters is indicative of

456 pressurisation within the upper conduit [12]. Crystal-rich magma forms a viscous cap in the upper

457 conduit that inhibits flow, leading to pressure build-up at shallow levels and edifice inflation [11]. The

458 magnitude and direction of tilt of the volcano flanks can be used to infer the magnitude and depth of the

459 pressure source. Using an isotropically pressurised model [14] or elastic half-space model [12, 41], the

460 depth of the pressure source is always less than 1000 m below the surface of the dome for SHV. Also,

461 the pressure source either needs to be very large or distributed over a large area [14]. Green and Neuberg

462 [13], following research by Beauducel et al. [42], suggest that surface deformations recorded by tilt-

463 meters could instead, or in addition, be from shear stresses within the upper conduit rather than a single

464 large pressure source. The SHV flank displacements are then consistent with the generation of shear

465 stresses beginning within the upper 100's metres of the conduit walls. However, Green and Neuberg

466 [13] emphasize that the vertical extent of the pressure source is unconstrained because tilt measurements

467 are insensitive to deep sources. Considering vertical traction along the conduit walls the location for the

468 tilt hypocentre is calculated to be approximately 400m and 600 m a.s.l., that suggests a shear stress

469 depth of 160 to 360m below the conduit exit, with traction values between 0.5 and 1.5MPa [13].  For

470 vertical traction to explain the recorded tilt requires a pressure gradient of $6.7 \times 10^4$ - $2.0 \times 10^5$ Pa/m along

471 an upper conduit segment 30m in diameter [13].

472

473 [Location of figure 6]

474

475 We use our conduit flow model to calculate the over-pressure within the conduit with shear bands for a

476 magma shear strength of $2 \times 10^5$ Pa (Fig. 6). Figure 6a shows the over-pressure profile along the conduit

477 length for flow in the conduit with shear bands and without shear bands (i.e. Hagen-Poiseuille flow).

478    The pressure difference in figure 6b corresponds to the over-pressure in the conduit for Hagen-Poiseuille

479    flow minus the over-pressure in the conduit with shear bands for the same magma chamber pressure.

480    Hence, what figure 6b shows is the redistribution in over-pressure along the conduit length due to the

481    development of shear bands. A positive pressure difference corresponds to a drop in pressure and

482    therefore flank deflation. Everywhere the pressure difference is less or equal (at the magma chamber and

483    conduit exit) to the initial over-pressure field, but the difference is most significant in the upper part of

484    the conduit. This is more clearly shown in figure 7 which shows the over-pressure gradient along the

485    conduit length for flow with shear bands minus that for Hagen-Poiseuille flow. Below the depth in the

486    conduit where shear bands exist, the over-pressure gradient increases due to an increase in extrusion rate

487    (from the presence of shear bands) but no change in viscosity. Above the depth where shear bands form,

488    the over-pressure gradient decreases to values of $4 \times 10^4$ Pa/m. Figure 8 shows a summary of all the

489    model results for a magma shear strength of $2 \times 10^5$ Pa showing the pressure difference maximum and the

490    depth of the maximum against magma chamber pressure. These values for the depth and magnitude of

491    the pressure change are comparable to those inferred at SHV during cyclic activity.

492

493    [Location of figure 7]

494

495    [Location of figure 8]

496

497    **5. Discussion**

498    Shear bands are simulated using a strain-localisation model to occur when the shear-stress equals the

499    magma shear strength of the magma. This can result in the generation of shear bands to depths of

500    approximately 700 m for low magma shear strengths ($2 \times 10^5$Pa) and high magma chamber pressures

501    (142.9MPa). These shear bands may be responsible for lava effusion along shear boundaries at the free

502    surface, because they extend directly from the conduit exit, and flank inflation/deflation. Geophysical

503    evidence for the depth of shear bands at SHV is not well constrained other than from the pressure source

504    responsible for the inflation and deflation of the volcano flanks. Green and Neuberg, [13] and Voight et

505    al. [12] calculate the depth of such pressure sources to be between approximately 160 to 510 below the

506    conduit exit, consistent with our modelled shallow shear bands depths and pressure change maximum.

507

508

509    The over-pressure in the upper conduit is significantly affected by the formation of shear bands, due to a

510    change in the viscosity and flow field altering the conduit resistance. Our model shows that the over-

511    pressure decreases in the upper conduit due to the formation of shear bands, corresponding to the

512    deflation of the flanks. We model a change in over-pressure gradient of up to $4\times10^4$ Pa/m in the upper

513    conduit and a maximum pressure change of 4.5MPa at depths up to 300m; magnitudes that can be

514    related to the change in the tilt experienced during inflation and deflation cyclic events. Enhanced

515    degassing and ash emissions are observed during the inflation maximum and deflation cycle from cracks

516    on the dome surface [12]. This may be due to the enhanced permeability from the formation of shear

517    bands that generate micro-fractures. However there may be a competition between the process of

518    enhanced permeability from fragmentation, and an enhanced extrusion rates suppressing gas-loss from

519    shear band development. Also, an increase in extrusion rate due to the formation of shear bands may be

520    the explanation for why the deflation period for the volcano flanks is commonly more rapid than the

521    inflation period. Given further model constrains/improvements, an observed change in extrusion rate

522    could be used to infer the shear strength of the magma within the conduit or the greatest depth that shear

523    bands penetrate to.

524

525    The conduit of a volcano initially begins as a dyke connected to the magma chamber, with cylindrical

526    conduit geometries only developing at shallow levels where the erosional capabilities of magma are

527    higher. The radius or width of the dyke for SHV at depth is estimated to be approximately 11 to 12 m

528    with an uncertainty of 7 m, when considering the ascent rates of hornblende [43]. Our model suggests

529    that there may be a greatest depth at which upper shear bands can reach, and this will be the greatest

530    depth at which significant conduit wall erosion will occur, when ignoring explosive decompression

531    effects. Due to over-simplifications used in our model we can't constrain this depth. But future models

532    that couple the change in the conduit radius with depth, and the feedback it will have upon magma

533    viscosity and extrusion rates, will allow for an estimate of the conduit plumbing at depth.

534

535    For lower magma shear strength values the depth of shear bands can be expected to increase, but will

536    only reach the depths at which LP seismicity occurs (~1500 m) for unrealistically low magma shear

537    strengths. Thus, it is hard to reconcile LP seismic signals directly to the depth of shear bands simulated

538    in our model. To form shear bands at the depth where LP events occur requires either a more complex

539    magma shear strength model, the conduit to narrow at depth allowing the strain-rate to increase, or both.

540    A magma shear strength model dependent upon pressure and magma crystallinity will be the focus of

541    future research [44].

542

543    All models have their limitations, and we make several simplifying assumptions that are likely to affect

544    models results. First, we have to rely upon a pressure change, via a dome collapse event, to trigger flow.

545    However, in reality the magma is extruded without any large pressure change or dome collapse event in

546    a continuous manner. Indeed, it was during periods of rapid magma extrusion ($>5m^3s^{-1}$) that the cyclic

547    seismic and deformation was primarily observed. Thus a transient model including the temporal

548    evolution of shear bands is required to fully understand the influence of shear bands upon magma flow,

549    pressure and the timescales involved in cyclicity. Second, because we consider a maximum crystallinity

550    in our models, this reflects flows at low extrusion rates. For flow at higher extrusion rates the viscosity is

551    likely to be lower due to crystallisation growth kinetics [19, 25]. This process may suppress the

552    development of shear bands, due to a lower viscosity, resulting in lower shear stresses at the conduit

553    wall although the crystallinity is likely to remain approximately in equilibrium at the wall. Finally,

554    neglecting vesicularity means that we don't consider a variable density, which is likely to give

555    quantitatively different results. Introducing vesicularity into the model will decrease the weight of the

556    magma column which is likely to increase the extrusion rate and push the depth of shear bands to deeper

557    levels within the conduit. However, simplifications were necessary for this model, but despite this model

558    results suggest that changes in pressure and velocity fields due to shear bands could be significant,

559    especially during tilt and seismic cycles in eruptive behaviour.

560

567

568    **7. References**

569    [1] E. S. Calder, R. Luckett, R. S. J. Sparks, B. Voight, Mechanism of lava dome instability and

570    generations of rockfalls and pyroclastic flows at Soufrière Hills Volcano, Montserrat, Geological

571    Society London Memoirs 21 (2002) 191 - 210.

572

573    [2] R. B. Watts, R. A. Herd, R. S. J. Sparks, S. R. Young, Growth patterns and emplacement of the

574    andesite lava dome at Soufrière Hills Volcano, Montserrat, Geological Society London Memoirs 21

575    (2002) 115 - 152.

576

577    [3] R. S. J. Sparks, S. R. Young, The eruption of Soufrière Hills Volcano, Montserrat (1995 - 1990):

578    overview of scientific results, Geological Society London Memoirs 21 (2002) 45 - 69.

579

580    [4] R. S. J. Sparks, M. D. Murphy, A. M. Lejeune, et al., Control on the emplacement of the andesite

581    lava dome of the Soufriere Hills volcano, Montserrat by degassing-induced crystallization. Terra Nova

582    12 (2000) 14-20.

583

584    [5] H. Tuffen, D. B. Dingwell, H. Pinkerton, Repeated fracture and healing of silicic magma generate

585    flow banding and earthquakes? Geology 31 (2003) 1089 – 1092.

586

587    [6] H. Kumagai, B. A. Chouet, The complex frequencies of long-period seismic events as probes of fluid

588    composition beneath volcanoes. Geophysical Journal International 138 (1999) F7-F12

589

590    [7] J. Neuberg, R. Luckett, B. Baptie, et al, Models of tremor and low-frequency earthquake swarms on

591    Montserrat, Journal of Volcanology and Geothermal Research 101 (2000) 83-104.

592

593    [8] B. Baptie, R. Luckett, J. Neuberg, Observations of low-frequency earthquakes and volcano tremor at

594    Soufrière Hills Volcano, Montserrat, Geological Society London Memoirs 21 (2002) 611 - 630.

595

596    [9] O. Jaquet, R. Carniel, R. S. J. Sparks, et al., DEVIN: A forecasting approach using stochastic

597    methods applied to the Soufriere Hills Volcano, Journal of Volcanology and Geothermal Research 153

598    (2006) 97-111.

599

600    [10] J. W. Neuberg, Tuffen, H, Collier, L, et al.,The triggering mechanism of low-frequency earthquakes

601    on Montserrat. Journal of Volcanology and Geothermal Research, 153 (2005) 37-50.

602

603    [11] K. Diller, A. B. Clarke, B. Voight, A. Neri, Mechanisms of conduit plug formation: Implications

604    for Vulcanian explosions. Geophysical Research Letters 33 (2006) L20302.

605

606    [12] B. Voight, R. S. J. Sparks, A. D. Miller, et al., Magma flow instability and cyclic activity at

607    Soufriere Hills Volcano, Montserrat, British West Indies. Science 283 (1999) 1138-1142.

608

609    [13] D. N. Green, J. Neuberg, Waveform classification of volcanic low-frequency earthquake swarms

610    and its implication at Soufriere Hills Volcano, Montserrat, Journal of Volcanology and Geothermal

611    Research 153 (2006) 51-63.

612

613    [14] C. Widiwijayanti, A. B. Clarke, D. Elsworth, B. Voight, Geodetic constraints on the shallow

614    magma system at Soufriere Hills Volcano, Montserrat, Geophysical Research Letters 32 (2005) L11309

615

616 [15] D. N. Green, J. Neuberg, V. Cayol,  Shear stress along the conduit wall as a plausible source of tilt

617 at Soufriere Hills volcano, Montserrat, Geophysical Research Letters 33 (2006) L10306

618

619 [16] J.-M. Bardintzeff, A. R. McBirney, Volcanology, Second ed., Jones and Bartlett Publishers,

620 Sudbury, Massachusetts, 2000.

621

622 [17] A. Costa, Viscosity of high crystal content melts: Dependence on solid fraction, Geophysical

623 Research Letters 32 (2005) L22308

624

625 [18] Hess K. U. and D. B. Dingwell Viscosities of hydrous leucogranitic melts: A non-Arrhenian

626 model. American Mineralogist 81 (1996): 1297 – 1300.

627

628 [19] O. E. Melnik, R. S. J. Sparks, Non-linear dynamics of lava dome extrusion. Nature 402 (1999) 37-

629 41.

630

631 [20] O. E. Melnik, R.S.J. Sparks, Dynamics of magma ascent and lava extrusion at Soufrière Hills

632 Volcano, Montserrat, Geological Society London Memoirs 21 (2002) 595 - 602.

633

634 [21] O. E. Melnik, R. S. J. Sparks, Controls on conduit magma flow dynamics during lava dome

635 building eruptions. Journal of Geophysical  Research, 110 (2005): doi:10.1029/2004JB003183.

636

637 [22] R. P. Denlinger, R. P. Hoblitt, Cyclic behaviour of silicic volcanoes, Geology 27 (1999) 459 – 462.

638

639    [23] J. J. Wylie, B. Voight, J. A. Whitehead, Instability of magma Flow from Volatile Dependent

640    Viscosity. Science 285 (1999) 1883 – 1885

641

642    [24] H. Massol, C. Jaupart, D. Pepper D, Ascent and decompression of viscous vesicular magma in a

643    volcanic conduit. Journal of Geophysical Research. 106 (2001):16223-16240.

644

645    [25] A. J. Hale, G. Wadge, H.-B. Mühlhaus, The Influence of Viscous and Latent Heating on Crystal-

646    Rich Magma Flow in a Conduit. Submitted to Geophysical Journal International.

647

648    [26] H. M. Gonnermann, M. Manga, Explosive volcanism may not be an inevitable consequence of

649    magma fragmentation, Nature 426 (2003) 432 – 435

650

651    [27] J. Barclay, M.J.Rutherford, M.R.Carroll, Experimental phase equilibria constraints on pre-eruptive

652    storage conditions of the Soufrière Hills magma, Geophysical Research Letters. 25 (1998) 3437 -- 3440.

653

654    [28] L. Moresi, F. Dufour, H.-B. Mühlhaus., Mantle Convection Modeling with Viscoelastic/Brittle

655    Lithosphere: Numerical Methodology and Plate Tectonic Modeling. Pure and Applied Geophysics. 159

656    (2002) 2335 - 2356

657

658    [29] H. B. Mühlhaus, I. Vardoulkis, The thickness of shear bands in antigranular-materials.

659    Geotechnique 37 (1987) 271 - 283

660

661  [30] R. A. Herd, M, Edmonds, V. A. Bass, Catastrophic lava dome failure at Soufriere Hills Volcano,

662  Montserrat, 12-13 July 2003, Journal of Volcanology and Geothermal Research 148 (2005) 234-252.

663

664  [31] R. S. J. Sparks, Causes and consequences of pressurisation in lava dome eruptions, Earth and

665  Planetary Science Letters. 150 (1997)177 -- 189.

666

667  [32] M. J. Rutherford, J. D. Devine, Magmatic conditions and magma ascent as indicated by hornblende

668  phase equilibria and reactions in the 1995-2002 Soufriere Hills magma, Journal of Petrology 44 (2003)

669  1433-1454.

670

671  [33] A. M. Lejeune, Y. Bottinga, T.W. Trull, P. Richet, Rheology of bubble-bearing magmas, Earth and

672  Planetary Science Letters. 166 (1999) 71 - 84.

673

674  [34] R. Pal, Rheological behavior of bubble-bearing magmas. Earth and Planetary Science Letters 207

675  (2003) 165-179.

676

677  [35] H. Pinkerton, R. J. Stevenson, Methods of determining the rheological properties of magmas at sub-

678  liquidus temperatures, Journal of Volcanology and Geothermal Research 53 (1992) 47-66.

679

680  [36] P. Kearey, F. J. Vine, 1996. Global Tectonics, Second edition, Blackwell Science.
681

682  [37] Mühlhaus, H-B and Regenauer-Lieb, K, Towards a self-consistent plate mantle model that includes

683  elasticity: simple benchmarks and application to basic modes of convection, Geophysical Journal

684  International. 163 (2) (2005) 788-800

685

686 [38] L. Gross, L. Bourgouin, A.J. Hale, H.-B. Mühlhaus, Interface Modeling in Incompressible Media

687 using Level Sets in Escript, Physics of The Earth and Planetary Interiors. In Press.

688

689 [39] A. J. Hale, L. Bourgouin, H. B. Mühlhaus, Using the level set method to model endogenous lava

690 dome growth, Journal of Geophysical Research, 112 (2007) B03213

691

692 [40] T. H. Druitt, S. R. Young, B. Baptie, et al., Episodes of cyclic Vulcanian explosive activity with

693 fountain collapse at Soufrière Hills Volcano, Montserrat, Geological Society London Memoirs 21

694 (2002) 218 – 306.

695

696 [41] J. B. Shepherd, R. A. Herd, P. Jackson, et al., Ground deformation measurements at the Soufriere

697 Hills volcano, Montserrat: II: Rapid static GPS measurements June 1996 June 1997, Geophysical

698 Research Letters 25 (1998) 3413-3416.

699

700 [42] F. Beauducel, P. Briole, J. L. Froger, Volcano-wide fringes in ERS synthetic aperture radar

701 interferograms of Etna (1992-1998): Deformation or tropospheric effect?, Journal of Geophysical

702 Research 105 (2000) 16391-16402.

703

704 [43] J. D. Devine, M. J. Rutherford, J. E. Gardner, Petrologic determination of ascent rates for the 1995-

705 1997 Soufrière Hills Volcano andesitic magma. Geophysical Research Letters, 25 (1998) 3669-3672.

706

707    [44] A. J. Hale. Magma Flow Instabilities in a Volcanic Conduit: Implications for Long-Period

708    Seismicity. Physics of the Earth and Planetary Interiors. In Press. DOI:10.1016/j.pepi.2007.05.001

709

710    [45] C. Romano, J. E. Mungall, T. Sharp, D. B. Dingwell, Tensile strengths of hydrous vesicular glasses:

711    An experimental study. American Mineralogist, 81 (1996) 1148 - 1154

712

713   **Figure captions:**

714   Figure 1: Schematic of a volcano, showing a conduit connecting the magma chamber to the free-surface,

715   with lava dome/flow at the conduit exit (not to scale). In reality the conduit may narrow at depth but it is

716   assumed to be a constant radius for simplicity in this model. Also shown is the approximate depth at

717   which LP seismicity and pressurisation responsible for volcano flank tilt occurs. Shown next to the

718   schematic is the model domain. We use axisymmetric coordinates, modelling the conduit between $r = 0$

719   to the conduit wall at $r = 15$m. The length of the conduit is 5000m. Boundary 1 has the condition of an

720   applied pressure, the magma chamber pressure, and Boundary 4 is at atmospheric pressure. Boundary 3

721   has the condition of no-slip and Boundary 2 is a symmetry boundary, ensuring no flow in the radial

722   direction.

723

724   Figure 2: Results from one simulation with a magma shear strength of $2\times10^5$Pa, a magma chamber

725   pressure of 132.2 MPa requiring a pressure change of 14.7MPa at the free surface. From left to right are

726   plots of velocity in the $X_3$-axis, strain-rate, shear stress, and shear stress divided by the magma shear

727   strength (effectively the plasticity) within the conduit. Shown is only half of the conduit, from the centre

728   of the conduit at $r=0$ (left side of image) to the conduit wall at $r=15$m (right side of image). The conduit

729   radius has been stretched in the figures by a factor of 30 to better visualise the results along the entire

730   5km length of the conduit. Where the shear stress divided by the magma shear strength is exactly equal

731   to unity shear bands develop. This corresponds to a shear band one element wide, flush against the

732   conduit wall, within the red zone of the figure. For this simulation a shear band of length of 413.5m

733   forms between the conduit exit and a depth of 413.5m.

734

735     Figure 3: A typical modelled crystal volume fraction (a) and viscosity (b) along the length of the

736     conduit. Most of the change in viscosity and crystallinity occurs in the upper-conduit due to the pressure

737     field.

738

739     Figure 4: Modelled shear band length against pressure in the magma chamber for magma shear strength

740     values of $2\times10^5$Pa (filled shapes) and $5\times10^5$Pa (unfilled shapes). For the same magma shear strength the

741     magma chamber pressure governs the depth of the shear bands due to its influence upon the extrusion

742     rate and viscosity.

743

744     Figure 5: a) shows the extrusion rate modelled with and without shear bands against the pressure in the

745     magma chamber. The model uses a magma shear strength of $2\times10^5$Pa for the solid shapes and $5\times10^5$Pa

746     for the unfilled shapes. The initial extrusion rate for no shear bands in the conduit is given by the

747     crosses. b) shows the modelled change in extrusion rate (given by the extrusion rate with shear bands

748     divided by extrusion rate without shear bands) using the same symbols for the different magma shear

749     strengths.

750

751     Figure 6: a) Shows the over-pressure in the conduit with depth for flow in the conduit without shear

752     bands (i.e. Hagen-Poiseuille flow) and with shear bands for a magma shear strength of $5x10^5$Pa (Flow

753     with shear bands). Both flow models have a magma chamber pressure of 132.55MPa. Also shown is the

754     difference in pressure between the two flow regimes with depth in the conduit, a depth of zero

755     corresponds to the conduit exit. A positive pressure difference corresponds a decrease in the over-

756     pressure along the conduit length, i.e. flank deflation. b) Difference in over-pressure along the conduit

757     due to the development of shear bands for different magma chamber pressures, shown in the legend, all

758     for dome collapse events equivalent to 7MPa and a magma shear strength of $5 \times 10^5$Pa.

759

760     Figure 7: Change in over-pressure gradient for flow with shear bands minus flow without shear bands

761     (i.e. Hagen-Poiseuille flow) along the conduit length for different magma chamber pressures, shown in

762     the legend, for dome collapse events equal to 7MPa and a magma shear strength of $2 \times 10^5$Pa. A positive

763     pressure-gradient corresponds to an increase in the pressure gradient due to the presence of shear bands,

764     whilst a negative pressure gradient corresponds to a decrease. A depth of zero corresponds to the conduit

765     exit.

766

767     Figure 8: Summary of a) over-pressure maximum (see Fig. 6) and b) the depth of the maxima (see Fig.

768     6) against magma chamber pressure for all the model runs for a magma shear strength of $2 \times 10^5$Pa.

769

770    Table 1: Parameters used in the model which are appropriate for the magma from Soufrière Hills

771    Volcano.

| Symbol | Parameter | Reference | Value |
|---|---|---|---|
| T | Initial Temperature | 32 | 1123°K |
| $\phi$ | Crystal volume fraction in chamber | 4 | 0.6 |
| $\rho$ | Density | 19 | 2350 kg.m$^{-3}$ |
| $P_0$ | Maximum over-pressure | 31 | 20 MPa |
| $\xi$ | Parameter in effective viscosity function | 21 | 8.6 |
| $\theta_0$ | Parameter in effective viscosity function | 21 | 1.4 |
| $\phi_0$ | Parameter in effective viscosity function | 21 | 0.69 |
| $\alpha_S$ | Solubility coefficient | 19 | 4.11 x10$^{-6}$ Pa$^{-1/2}$ |
| $a_T$ | Liquidus and solidus coefficients | 21 | 1465.4 |
| $b_T$ | Liquidus and solidus coefficients | 21 | -31.4 |
| $c_T$ | Liquidus and solidus coefficients | 21 | -2.8 |
| $d_T$ | Liquidus and solidus coefficients | 21 | -0.41 |
| $R_C$ | Conduit radius | 27 | 15 m |
| $L_C$ | Conduit length | 27 | 5000m |
| $g$ | Acceleration due to gravity | | 10 m.s$^{-2}$ |

772

773    Table 2: Magma shear strength values quoted in the literature for lavas that are appropriate to our study.

| Magma Shear Strength | Reference | Comments |
|---|---|---|

| | | |
|---|---|---|
| $10^6 - 10^7$ Pa | 45 | Experimental results from hydrous vesicular glasses. |
| $10^6$ Pa | 12 | From estimates for the strength of lava from the height of spines extruded at Soufrière Hills Volcano, Montserrat. |
| $10^7$ Pa | 26 | Used in numerical models for magma fragmentation. |
| $0.5 - 1.5 \times 10^6$ Pa | 15 | Inferred from numerical models for the amplitude of tilt measured at Soufrière Hills Volcano, Montserrat. |
| $10^7$ Pa | 10 | Used in numerical models of magma flow at Soufrière Hills Volcano, Montserrat. |
| $10^7 - 10^8$ Pa | 5 | Magma shear strength values from laboratory experiments. |

774

775

776

777    Figure1:
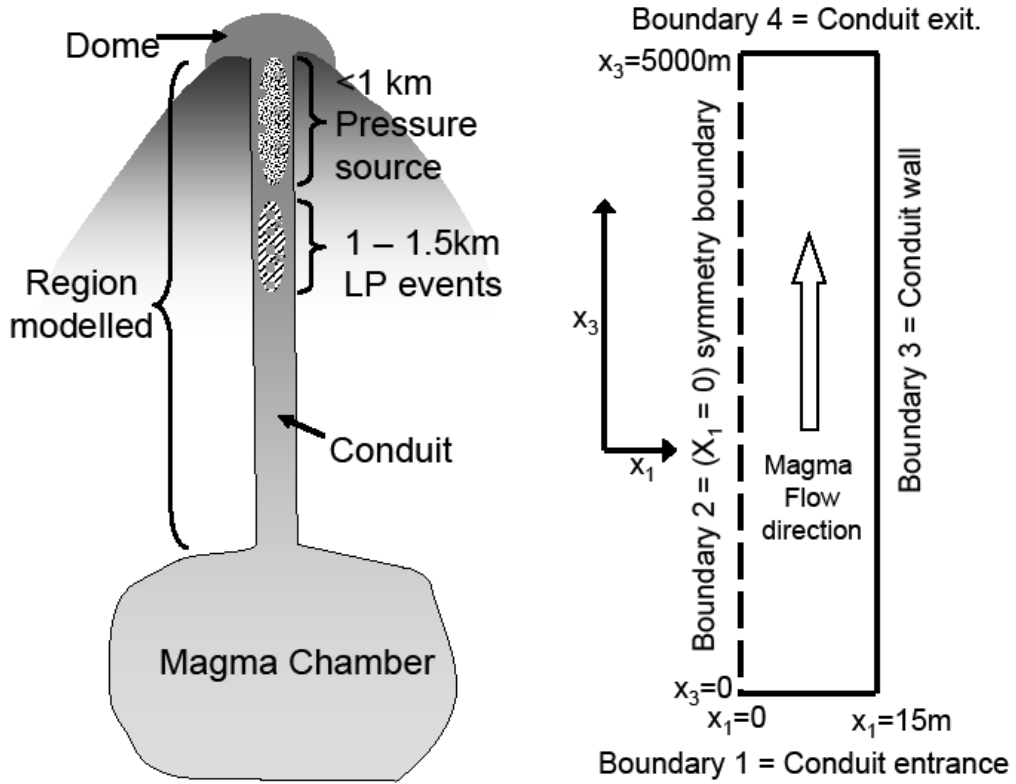


778

779

780

781    Figure2:
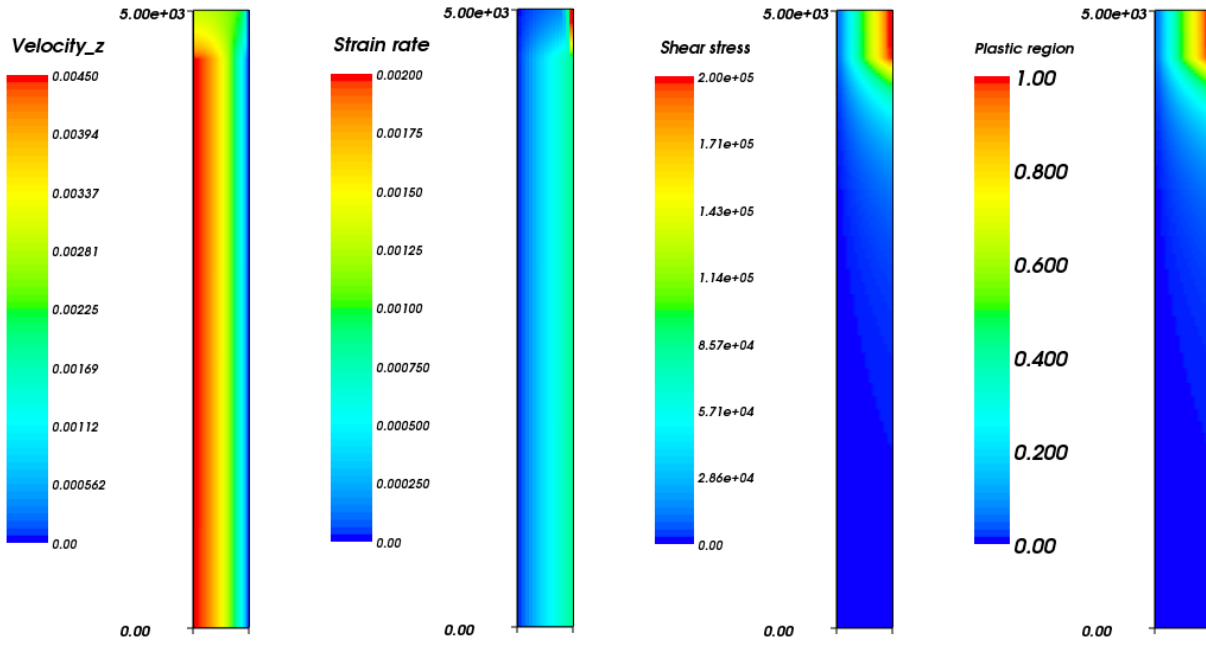


782

783

784     Figure 3:
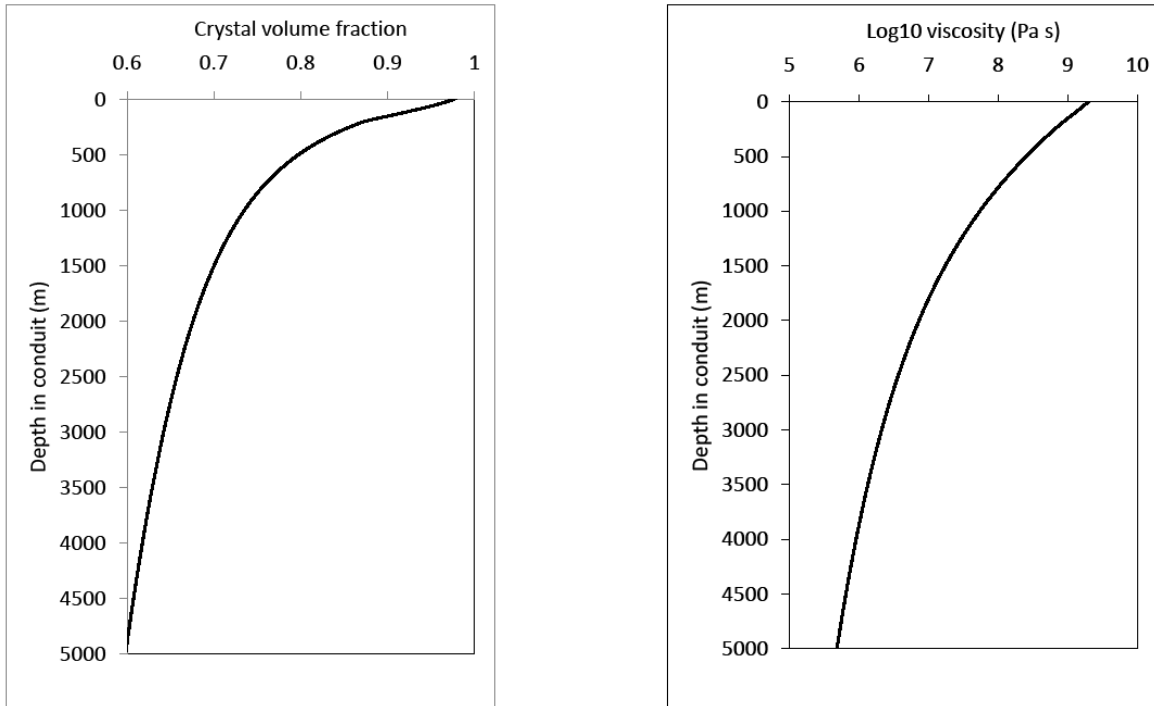


785

786

787    Figure 4:
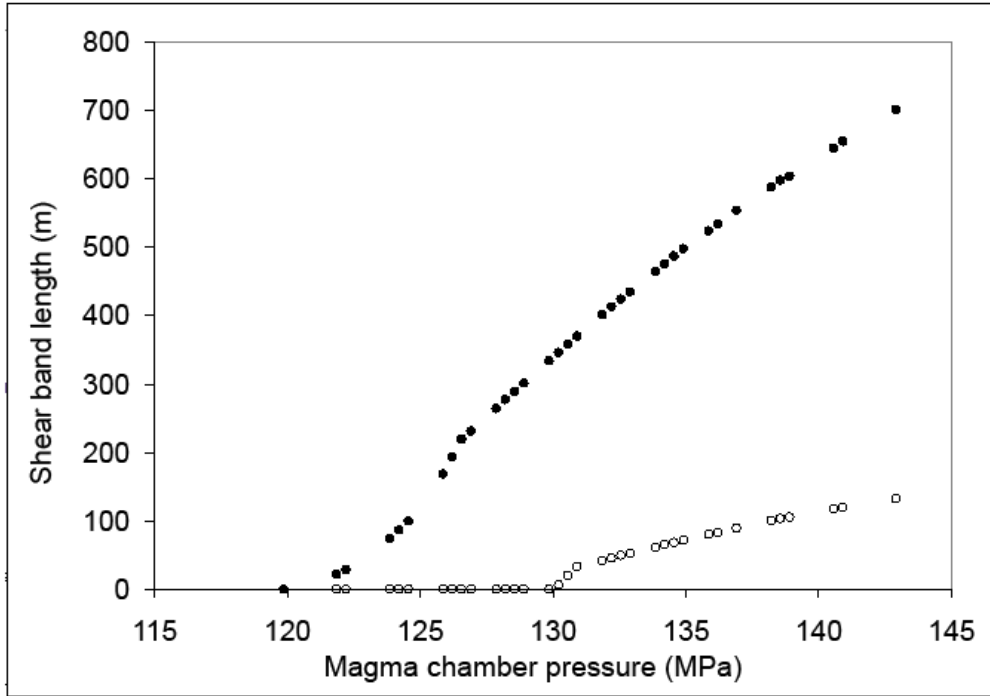


788

789

790    Figure 5a:



791

792    Figure 5b:



793
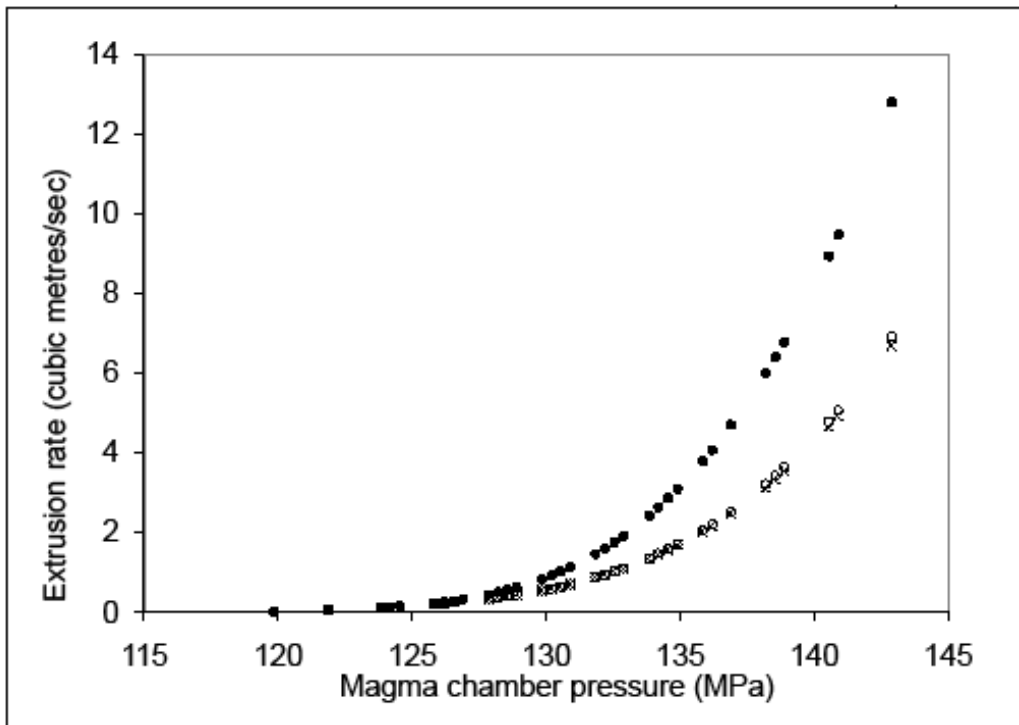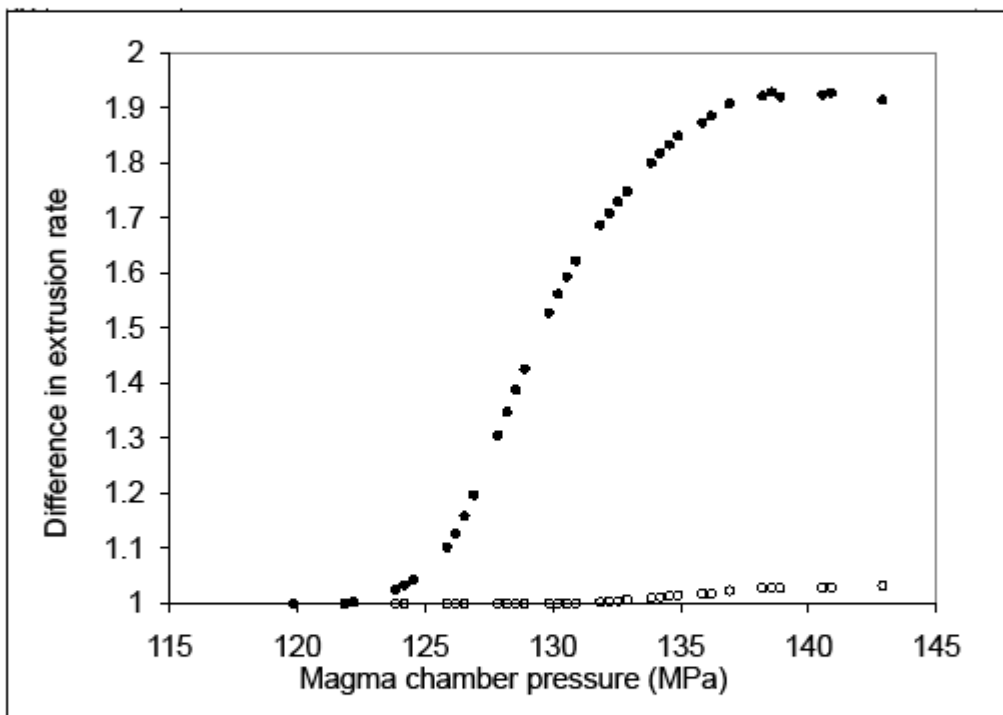
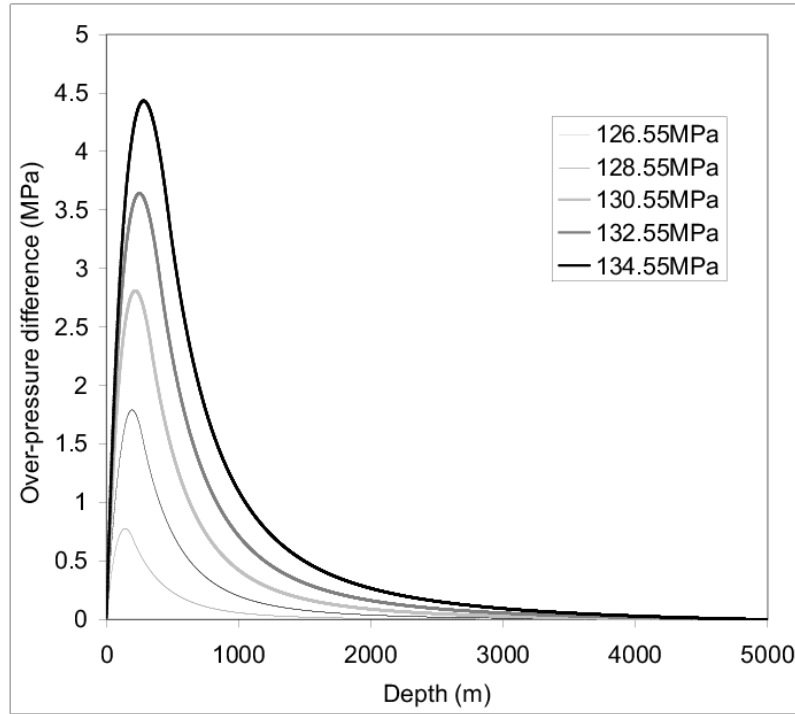794    Figure

795    6a:
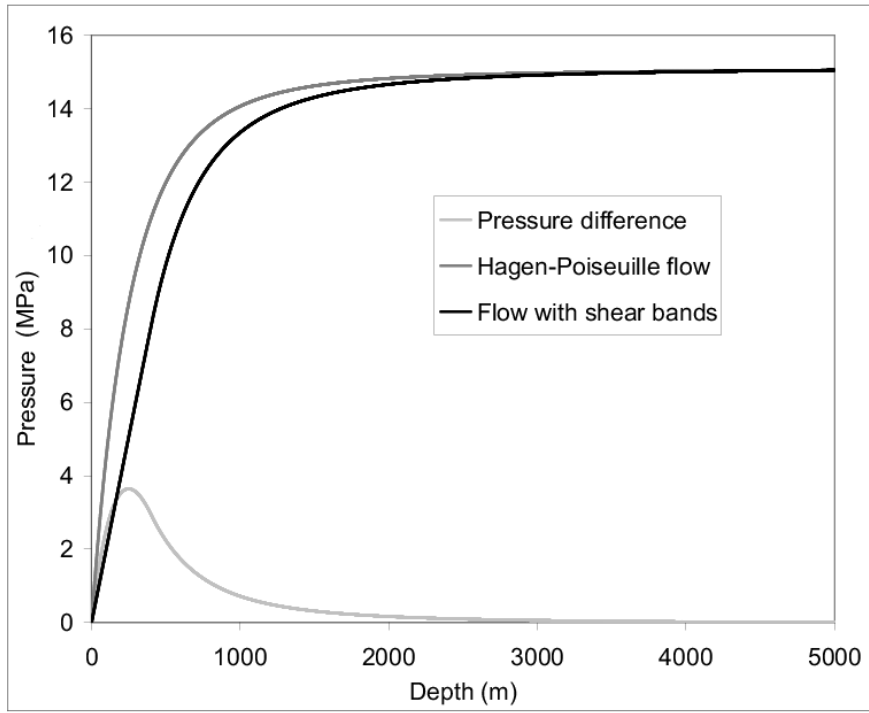


796
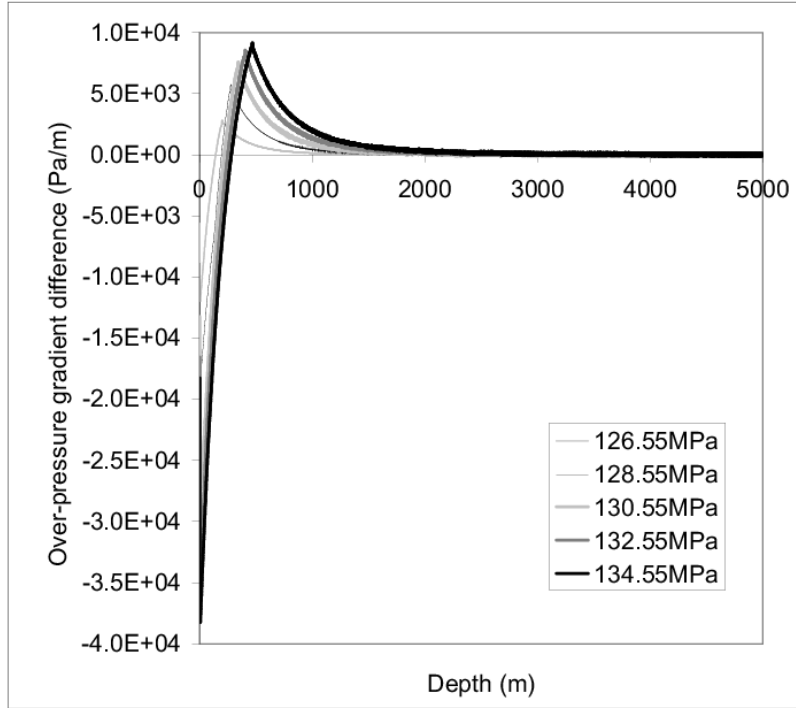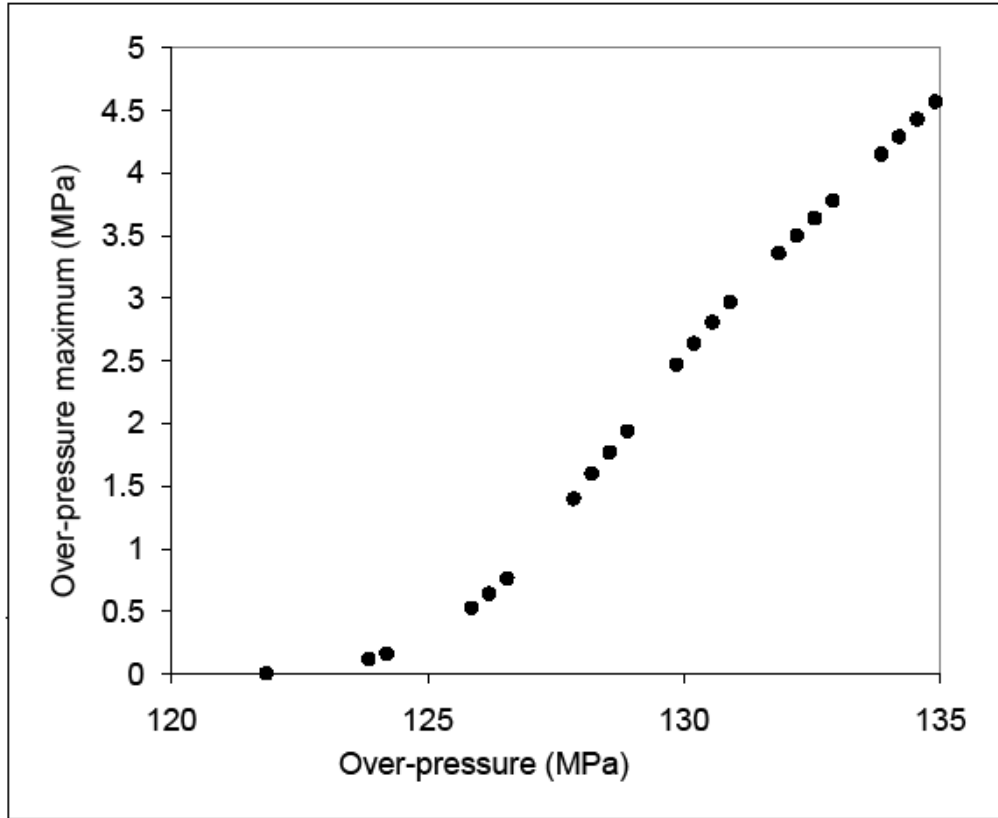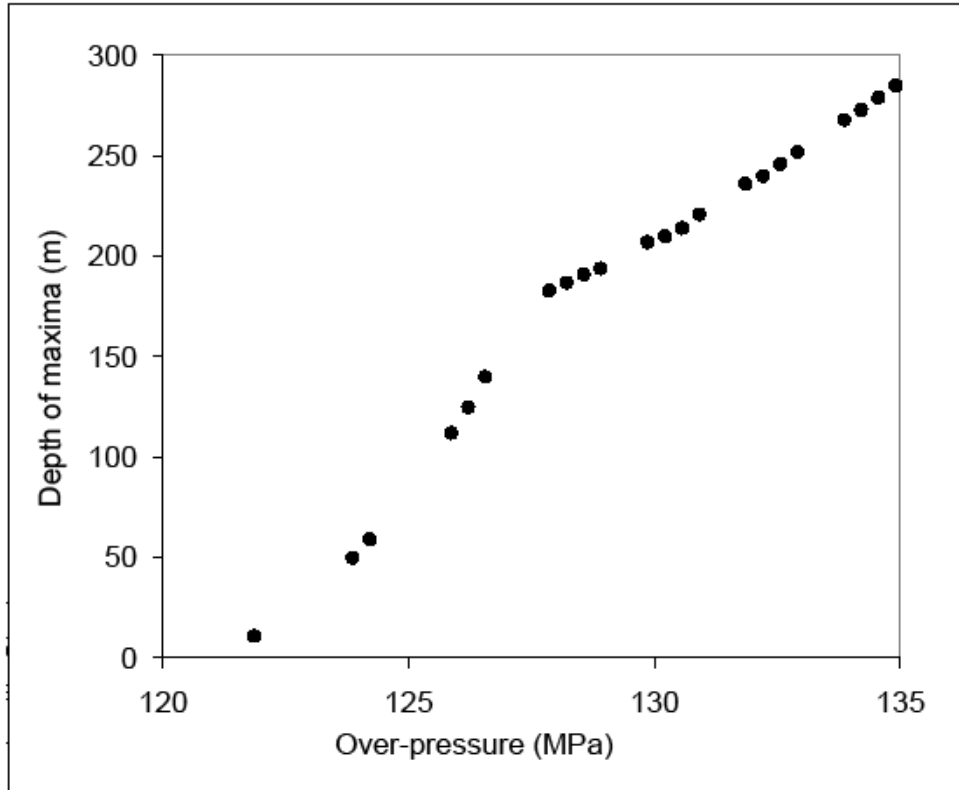
797

798     Figure 6b:



799

800

801    Figure 7:



802

803

804    Figure 8a:



805
806

807

808    Figure 8b:



809
810